Spectrochimica Acta Part B 65 (2010) 33–45

Contents lists available at ScienceDirect

Spectrochimica Acta Part B

journal homepage: www.elsevier.com/locate/sab

Resonantly laser induced plasmas in gases: The role of energy pooling and exothermic collisions in plasma breakdown and heating ☆

Cedomil Vadla [a], Vlasta Horvatic [a,*], Damir Veza [b], Kay Niemax [c]

[a] Institute of Physics, Bijenicka 46, 10000 Zagreb, Croatia
[b] Department of Physics, Faculty of Science, University of Zagreb, Bijenicka 32, 10000 Zagreb, Croatia
[c] ISAS-Institute for Analytical Sciences at the Technical University of Dortmund, Bunsen-Kirchoff-Str. 11, D-44139, Dortmund, Germany

ARTICLE INFO

Article history:
Received 8 June 2009
Accepted 24 October 2009
Available online 1 November 2009

Keywords:
Laser-produced plasma
Resonance pumping
Resonant LIBS

ABSTRACT

The present work is a systematic experimental study of the plasma formation in cesium vapor induced by a continuous laser tuned to the resonance transition $6S_{1/2}$–$6P_{3/2}$. Taking into account the measured absolute population densities of Cs ground and excited state atoms as well as the electron densities derived from Stark broadening of the Cs lines, complete local thermodynamic equilibrium in the laser-produced plasma was found for laser power densities $\approx 10\,\mathrm{Wcm}^{-2}$ at cesium ground state number densities of about $10^{17}\mathrm{cm}^{-3}$. Direct conversion of the excitation energy or parts of the excitation energy in exothermic collisions of laser-excited atoms is concluded to be the major process for atomic vapor heating and subsequent formation of LTE plasmas.

1. Introduction

There are still many open questions concerning plasma breakdown and evolution when laser radiation is absorbed by matter. Answers to these questions are not only important for better understanding and theoretical description in physics but also in applications where laser plasmas are produced, such as in material processing and coating, or chemical analysis. The present status of understanding can be taken from recent textbooks and reviews [1–3]. Although the detailed processes are depending strongly on the laser power density, pulse length and wavelength, there is the common denominator that electrons are key players in plasma breakdown and plasma heating since they absorb and distribute the laser energy in the plasma. Furthermore, there is consensus that it needs free electrons first, e.g., by single or multi-photon ionization of atoms or molecules, before they are heated by inverse Bremsstrahlung and transfer the energy by collisions to the heavy partners in a gas or solid.

The results of the present work indicate that an additional process is very important for heavy particle heating and plasma generation in a resonantly pumped vapor or gas. This particular process is based on exothermic collisions of the excited atoms with other atoms which increase the kinetic energy of the collision complexes and lead to hot plasmas with electron densities which correspond to the plasma temperatures.

Cs is used as a model vapor because it is easy to generate at moderate temperature, contains only about 0.5% molecules [4] at temperatures up to 600 K, has a low lying resonance state which can be directly populated by laser radiation by diode lasers (852.3 and 894.6 nm) and an ionization energy which is about three times the energy of the resonance state, important to control two-photon ionization from the ground state through the resonance state. Furthermore, the atomic transition probabilities of bound–bound, bound–free and free–free transitions as well as the Stark broadening parameters of the spectral lines are well known from experiment or from theoretical treatment of the relatively simple one-electron, hydrogen-like atom. The knowledge of these atomic parameters is necessary for plasma analysis by spectroscopy.

Resonant laser pumping of pure metal vapors and plasma production has been extensively studied from 1970 until 1990. Measures investigated the possibilities to enhance the electron density and the temperature in potassium plasmas by resonant laser absorption in a theoretical paper [5]. The first plasma production was observed by Lucartorto and McIlrath who pumped the Na D1 line with a pulsed dye laser [6]. A little later [7], Measures came up with an explanation for the surprisingly high population densities of excited Na states and the ionization process observed by Lucartorto and McIlrath. He argued that high-energy electrons created by super-elastic collision between electrons and atoms in excited states are responsible for the effective energy distribution process and are more important for ion production than non-resonant two-photon ionization from the resonantly pumped Na vapor. The idea of superelastic electron collisions was followed in a further experimental paper by

☆ The work was performed within the network "Plasma–Analyte Interaction Working Group (PAIWG)". The PAIWG is a collaborative effort of University of Florida (UF) in Gainesville, Bundesanstalt für Materialforschung und -prüfung (BAM) in Berlin, and ISAS in Dortmund, jointly funded by National Science Foundation and Deutsche Forschungsgemeinschaft.

* Corresponding author. Tel.: +385 1 469 8861; fax: +385 1 469 8889.
E-mail address: blecic@ifs.hr (V. Horvatic).

0584-8547/$ – see front matter © 2009 Elsevier B.V. All rights reserved.
doi:10.1016/j.sab.2009.10.010

the group of Menard and Measures [8] where plasma was created by one- and two-photon pumping of Sr vapor. A comprehensive experimental study of ionization and excitation of high-lying states in Cs by laser pumping of the second principal series lines (455.7 and 459.4 nm) was published by Huennekens et al. [9]. Also this paper favors superelastic electron collisions as the dominating process for plasma generation.

In the present experiment, the laser absorption of the Cs D2 line and the cesium vapor density are varied to investigate their influence on the production of free electrons and the population densities of excited Cs states. The excited vapor approaches to complete LTE condition with increasing optical pumping and Cs number density as will be shown in Section 3. Such behavior cannot be explained either by photoionization or by avalanche production of hot electrons by superelastic collisions. Therefore, exothermic collisions of excited atoms are proposed as major vapor heating mechanism.

Originally it was planned to populate high-lying nD_J levels of Cs with two resonant lasers via the resonance lines in order to study the satellites in the far wings of the self-broadened nD_J–$6P_J$ lines by fluorescence. The existence and the position of these satellites are verifying the magnitudes of extrema in the interaction potentials of large Rydberg molecules of the type $Cs^*(nD_J)+Cs(6\,S_{1/2})$ [10]. However, to our surprise the second laser step had no enhancement effect on the line which could be already detected by emission without the second laser step. An LTE plasma had been generated by laser pumping of the resonance transition $6S_{1/2}$–$6P_{3/2}$ at relatively low power.

We like to point out that resonant heating of free atoms may also be important in resonant laser ablation and resonantly laser induced breakdown spectrometry (resonance LIBS, see, e.g., [11–16]) which is used to enhance the signal to noise ratio of the line of the host atom in the plume by tuning the laser wavelength to the host atom resonant transition.

2. Experiment

The experimental arrangements used are schematically shown in Fig. 1. The Cs vapor was generated in a Pyrex glass tube-like cell with flat windows placed in an oven. The tube diameter was 20 mm and its length was 60 mm. The thickness of tube wall and the windows was 2 mm each. The cell was carefully backed under vacuum conditions in order to avoid any influence of foreign gas in the experiment. After cooling, the cell was filled with pure Cs metal and sealed under vacuum conditions by melting the glass tube connector to the pump. The Cs pressure was adjusted by varying the metal bath temperature in a "cold finger", not shown in Fig. 1. The temperature of the main body of the glass cell was kept slightly higher than the temperature of the cold finger ($\Delta T \sim 15$ °C) in order to avoid metal coating of the optical windows.

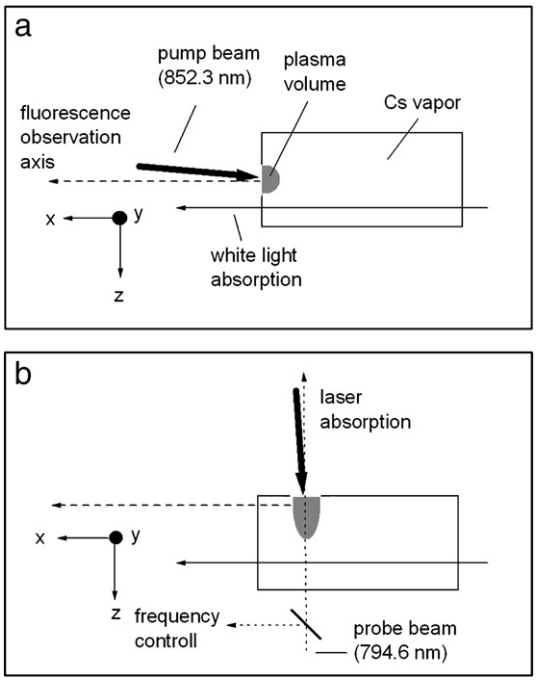

Fig. 1. Experimental arrangements for the first (a) and the second (b) parts of the experiment.

The Cs vapor was pumped by the D2 line ($6\,S_{1/2}$–$6P_{3/2}$, 852.3 nm) applying a tunable single mode laser diode. The power of the laser diode was varied in the range 50–80 mW.

In the first part (hereafter labeled with M0) of the experiment (see Fig. 1a), the laser beam entered the cell nearly perpendicular through the one of the windows. The beam was focused by a lens with the focal length $f=12.5$ cm. The focus was placed just behind the window at the position for which the backward measured fluorescence had a maximum. The measurements were performed in the cesium density range from $4\times10^{16}\,cm^{-3}$ to $1\times10^{17}\,cm^{-3}$. The cesium number density N_{Cs} was measured using the white light absorption in the quasistatic wings of the Cs D2 line [17]. The wavelength of the laser beam was tuned in the blue wing close to the center of the Cs D2 line. The laser wavelength was controlled by a laser wavemeter (Burleigh). Laser detuning was chosen so as to get maximum resonance fluorescence, i.e. an optimum of the Cs atoms excited to the $6P_{3/2}$ state. For instance, at cesium number density $N_{Cs}=10^{17}\,cm^{-3}$, the maximum fluorescence was achieved with laser detuning $\Delta\lambda=0.06$ nm. In that case, the laser beam was strongly absorbed and the excited vapor was restricted to a small bright volume (size: about 1×1 mm) just behind the cell window. The central part of the fluorescence volume was imaged onto the entrance slit (width: 70 μm, height: 300 μm) of a 1 m McPherson monochromator (grating: 1200 grooves/mm). The slit height was limited by an aperture to get sufficient spatial resolution. The excitation volume was imaged with 1.9 magnification applying a quartz lens ($f=11$ cm). The wavelength dependent, relative detection sensitivity of the spectroscopic system (monochromator, imaging lens and RCA C31034 photomultiplier) was calibrated by a standard tungsten ribbon lamp to allow quantitative intensity measurements. Typical emission spectra obtained are shown in Fig. 2.

The data analysis, presented in the next section, showed that the produced plasmas at optimum pumping conditions were in complete LTE. Plasma temperatures between 2400 K and 2500 K were achieved at cesium number densities in the range from $5\times10^{16}\,cm^{-3}$ to $10^{17}\,cm^{-3}$ and optimum laser detuning in blue wing of the Cs D2 line of 0.04 nm and 0.07 nm, respectively.

To get more information about the mechanism of plasma generation by resonant laser induced breakdown, the spatially resolved spectra were recorded in the second part of the experiment. In particular, the stepwise transition of the plasma to the LTE conditions was investigated. The measurements were performed at lower cesium number than in the previous experiment. The laser detuning $\Delta\lambda_L$, the power W_0 as well as the beam diameter r_0 were varied. Here, the beam diameter is defined as full width at half maximum of the laser beam intensity profile. The basic parameters of the performed set of measurements are listed in Table 1.

The laser beam entered the cell through the curved tube wall near to one of the windows as shown in Fig. 1b. The spectra were measured side-on at the position where the fluorescence has a maximum, i.e., close to the cell wall ($z=0$). The imaging geometry used was the same as in the previous experiment. In this manner, the observed volume was restricted to a long thin column (cross section of about $150\times35\,\mu m^2$) along the x-axis. Different volumes of the laser-produced plasma could be measured by translating the imaging lens in the y- and z-directions.

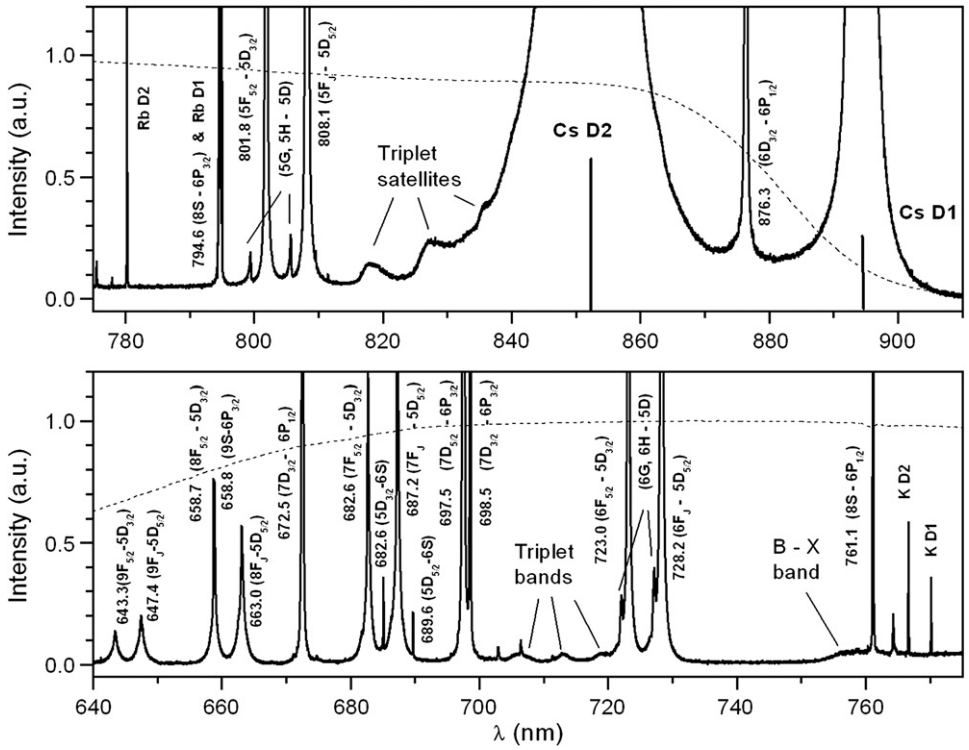

Fig. 2. Typical emission spectra obtained by cw laser pumping of the D2 resonance state at a Cs density of $N_{Cs} = 10^{17}\,cm^{-3}$ (M0 measurement). The laser wavelength was tuned $\Delta\lambda = 0.07$ nm from the line center into the blue wing of the Cs D2 line. The laser power was 80 mW. The dashed lines represent the spectral response ε_λ of the detection system.

The excitation volume was radially symmetric with respect to the z-axis. The radial distributions of the excited atoms were measured by moving the imaging lens in the y-direction. The spatial distributions of the Cs atoms in the resonant $6P_J$ states were determined by the measurements of the spatially dependent fluorescence intensities in the optically thin wings of the Cs D2 and D1 lines. For this purpose, the monochromator was tuned about 2–3 nm either in the blue wing of the Cs D2 or red wing of the Cs D1 line. In the same manner, the spatial distributions of cesium atoms excited to the higher states were determined by measuring the peak intensities of the corresponding optically thin spectral lines. Typical radial distributions measured at $z = 0$ at two different experimental conditions are shown in Fig. 3. The intensity distribution $F_0(y)$ of the laser beam was determined by the measurement of the resonance fluorescence distribution at very low cesium number density ($N_{Cs} \approx 10^{11}\,cm^{-3}$ at cell temperature slightly above room temperature). It was shown that, the distributions $F_{D1}(y)$ and $F_{D2}(y)$ of cesium atoms in $6P_{1/2}$ and $6P_{3/2}$ states, respectively, show no mutual difference within the experimental error, but they are generally broader than the $F_\lambda(y)$ distributions of Cs atoms in higher excited states. However, the Cs $6P_J$ distributions were closer to the distributions in the higher excited states when the Cs ground state number density was increased at comparable pumping. At given experimental conditions, the distributions of cesium atoms in higher excited states are practically of the same shape. As a representative of the number density distributions in higher excited states, the intensity distribution of the Cs $5D_{5/2} \rightarrow 6S_{1/2}$ quadrupole transition at 685 nm is given in Fig. 3.

Laser absorption measurements were performed to get quantitative information on the population in the Cs $6P_{3/2}$ state. The absorption of the $6P_{3/2}$–$8S_{1/2}$ transition at 794.6 nm was measured along the

Table 1
Parameters in the first (M0) and in the second (M1–M7) part of the experiment.

Measurement code	W_0 (mW)	$\Delta\lambda_L$ (nm)	r_0 (mm)	N_{Cs} ($10^{16}\,cm^{-3}$)
M0	80	0.06	0.03	10
M1	50	0.08	0.05	0.81
M2	50	0.04	0.05	0.81
M3	80	0.04	0.03	0.57
M4	80	0.05	0.05	1.62
M5	80	0.04	0.03	1.84
M6	60	0.04	0.03	3.9
M7	80	0.04	0.03	3.9

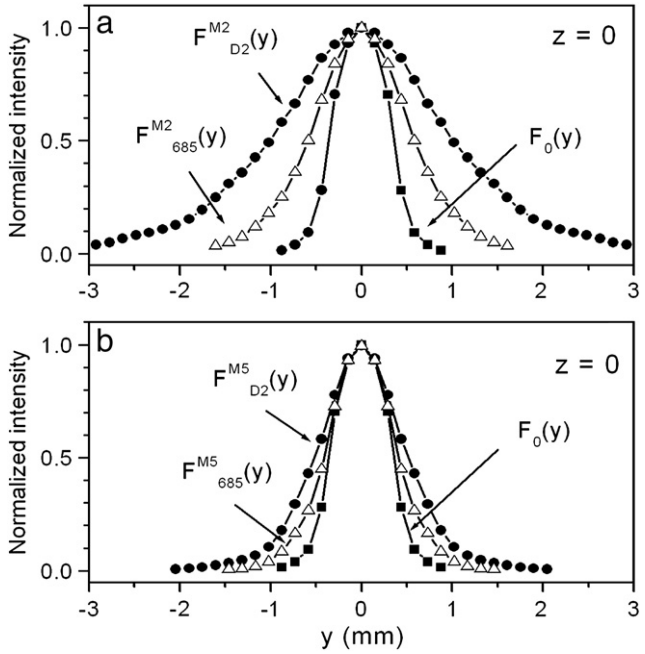

Fig. 3. Normalized spatial distributions $F_{D2}(y)$ of the Cs D2 line wing intensity and the intensity distributions $F_{685}(y)$ of the Cs $5D_{5/2} \rightarrow 6S_{1/2}$ quadrupole line at 685 nm. The $F_0(y)$ is the intensity distribution of the pump beam. The distributions in (a) and (b) parts of the figure were obtained at experimental conditions labeled as M2 and M5 in Table 1, respectively. The distributions were measured at the position z = 0 (close to the cell wall).

z-axis in the central part of the axially symmetric excitation volume (see Fig. 1b). For this purpose, second single mode, tunable laser diode with collimated beam (diameter: ~200 μm) was used. The laser power density was attenuated by optical filters to $<100\ \mathrm{nW/cm^2}$ to avoid optical saturation of the probed atoms. The transmitted light was detected by a silicon photodiode and the dispersion of the diode laser absorption spectra was determined by measuring simultaneously the transmission peaks of a confocal Fabry–Perot interferometer (free spectral range: 2 GHz). Typical laser absorption spectra are shown in Fig. 4a. In addition, the spatial distributions $F_{D2}(z)$ of the Cs D2 fluorescence intensities were measured. $F_{D2}(z)$ for two different experimental conditions (M2 and M5 in Table 1) are displayed in Fig. 4b. As can be seen in Fig. 4., the spatial distributions of the excited atoms in the present experiment are strongly inhomogeneous due to very strong absorption of the excitation laser beam tuned close to the Cs D2 line center. Therefore, the spectra were measured at a position close to the point where the pump beam entered the vapor cell as already mentioned before.

3. Data analysis and results

3.1. First part of the experiment: strong pumping at high number densities

The experimental configuration used in the first part of the experiment is shown in Fig. 1a. It allowed the determination of the relative populations of cesium atoms in the excited states. Quantitative analysis conducted in the second part of the measurements confirmed that all emission lines, except the first two resonance 6S-nP doublets, were optically thin in all experimental conditions applied. Therefore, the measured integral emission intensities of all recorded lines of the diffuse (nD_J–$6P_J$), sharp ($nS_{1/2}$–$6P_J$) and Bergmann series (nF_J–$5D_J$) can be expressed as:

$$I_{mn} \propto \varepsilon(\lambda_{mn}) h\nu_{mn} N(m) A_{mn}. \tag{1}$$

where $\varepsilon(\lambda_{mn})$ denotes the response of the detection system at the considered wavelength.

In the evaluation of the results the values of the spontaneous emission coefficients A_{mn} taken from [18] were used. Statistically weighted populations $N(5D)/g(5D)$ were arbitrarily chosen to be equal to 1, and relative statistically weighted populations $N(nL)/g(nL)$ in S, other D, and F states were evaluated via Eq. (1) relatively to the statistically weighted populations in the Cs $5D_J$ state. Here, the integral intensity ratios of the relevant spectral lines and the quadrupole lines at 685 nm and 696 nm ($5D_J \rightarrow 6S_{1/2}$ transition) were used. The values for the spontaneous emission rates of these quadrupole lines were taken from [19]. The relative populations in the resonant $6P_J$ state could not be determined in this way for two reasons. The kernels of the resonance lines were optically thick, and the spontaneous emission rates are significantly lowered due to radiation trapping. However, as shown in [20], the quasistatic wings of alkali resonance lines can be used as an accurate relative standard of radiation. The registered fluorescence intensity in the red and blue wings at detuning Δλ from the D1 and D2 line centers, respectively, can be written as:

$$I_J(\Delta\lambda) \propto \varepsilon(\lambda_J) h\nu_J N(6P_J) A_J(\Delta\lambda). \tag{2}$$

The spontaneous emission rates $A_J(\Delta\lambda)$ for the relevant self-broadened quasistatic resonance line wings are given by [20]:

$$A_J(\Delta\lambda) = N(6S)\frac{\delta\lambda}{(\Delta\lambda)^2}\beta_J(\Delta\lambda). \tag{3}$$

Here, $\delta\lambda$ is the monochromator band-pass and β_J are detuning-dependent coefficients. In the case of detuning which is small compared with the fine structure splitting, the coefficients $\beta_{1/2}$and $\beta_{3/2}$ for Cs D1 and Cs D2 lines are nearly constant and amount to $0.43\,\mathrm{cm^3 s^{-2}}$ and $0.68\,\mathrm{cm^3 s^{-2}}$, respectively Therefore, the intensity ratios of optically thin line wings and optically thin lines allow determination of the relative populations in the resonant $6P_J$ states. For instance, the relative population in the $6P_{3/2}$ with respect to the population in the $5D_{5/2}$ state can be determined by using the following relation:

$$\frac{N(6P_{3/2})}{N(5D_{5/2})} = \frac{1}{N(6S)}\frac{852}{685}\frac{\varepsilon_{685}}{\varepsilon_{852}}\frac{A_{685}}{\beta_{3/2}}\frac{(\Delta\lambda)^2}{\delta\lambda}. \tag{4}$$

No measurable difference between relevant spatial intensity distributions (in y or z-direction) was found in this part of the experiment. Therefore, the corresponding spatial distribution factors do not appear in Eqs. (3) and (4). However, the measured intensities are related to average values along the x-axis. It was supposed that spatial distributions in that direction are equal too. In order to use Eq. (4), the cesium ground state number density has to be known. In the present experiment, the Cs ground state number density was measured outside the excitation volume. It was determined from the white light

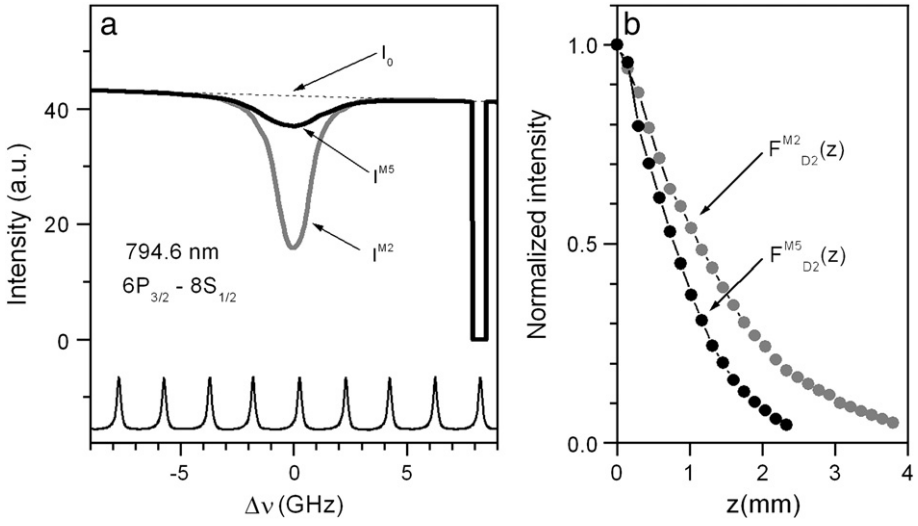

Fig. 4. (a) Laser absorption spectra obtained in the measurements M2 and M5 (see Table 1) together with the transmission peaks of the Fabry–Perot interferometer with 2 GHz FSR (lower trace). (b) The corresponding intensity distributions $F_{D2}(z)$ in the optically thin wing of the Cs D2 line.

absorption (see Section 1.) along the cell in the x-direction. The evaluation of the spectra shown in Fig. 2 yielded almost perfect Boltzmann plots, which is shown in Fig. 5.

All data in Fig. 5 which belong to the $5D_J$ and higher states are on a straight line represented by $\exp(-E/k_B T_{exc})$, where $T_{exc} = (2540 \pm 50)$ K. Calculation reveals that the number density of the excited cesium atoms N_{Cs}^* amounts to only a few percent of the total atom number density if an excitation temperature of 2540 K is taken into account. This means that the ground state atom number density $N(6S)$ is approximately equal to the total number density N_{Cs}. This estimate is very important for the evaluation of the populations in the resonance states. The relative $N(6P_J)/g(6P_J)$ values, calculated according to Eq. (4) and using the cesium number density measured outside the excitation volume, yielded values which were obviously lower than expected from the extrapolation of the Boltzmann plot (see Fig. 5 and inset). The measured cesium ground state number density outside the excitation volume was $N_{Cs}^{out} = (1 \pm 0.05) \times 10^{17}\,cm^{-3}$ and the vapor temperature T_a^{out} was about 610 K. However, if Eq. (4) is evaluated using a four time lower $N(6S)$ values (accuracy: ±10%), the corresponding corrected values of $N(6P_J)/g(6P_J)$ lie on a straight line together with all other states in the Boltzmann plot (see inset of Fig. 5). The fitted cesium number density for the laser excitation volume $N_{Cs}^{in} = (2.5 \pm 0.3) \times 10^{16}\,cm^{-3}$ yields a temperature of $T_a^{in} = (2400 \pm 300)$ K if Dalton's law is applied. This value is in excellent agreement with the excitation temperature, supporting the conclusion that the excited cesium plasma is in the LTE.

The LTE statement is additionally confirmed by the values of electron number density, which were obtained from the Stark broadening of the Cs $nF_J \rightarrow 5D_J$ lines taking into account the data of Agnew [21] based on the Stark broadening theory of Griem [22]. The Stark broadening data have been verified by several experiments (see [9]). In Fig. 6 the Stark broadening of two Cs Bergmann series lines ($9F_J \rightarrow 5D_J$ and $7F_J \rightarrow 5D_J$) is demonstrated. The spectra are taken from the overview spectrum displayed in Fig. 2. Since the full width at half maximum (FWHM) of the considered lines is much broader than the FWHM of the instrumental profile $\delta\lambda$ of the monochromator (which can be approximately taken from the profile of the quadrupole lines $5D_J \rightarrow 6S$ at 685.0 and 689.7 nm), the Stark widths can be directly taken from the spectra for the determination of the electron density. For example, the FWHM of the 647.4 nm line is about 1.05 nm in Fig. 6 which, after taking into account the instrumental width $\delta\lambda \approx 0.08$ nm,

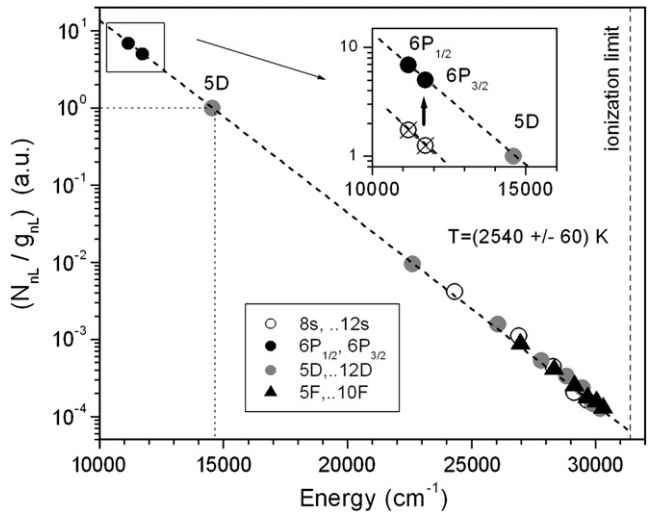

Fig. 5. Statistically weighted relative populations in the excited $6P_J$, nS, nD_J and nF_J states versus excitation energy. The data were obtained from the spectrum shown in Fig. 2 (M0 measurement). Inset: The non-corrected relative populations in the $6P_J$ states (crossed open circles) and the corrected values (full circles) assuming an about four times lower cesium ground state number density than measured outside of the excitation volume. See text for further explanations.

yields an electron number density $N_e = 3.9 \times 10^{14}\,cm^{-3}$ with a statistical accuracy of 10%.

LTE in plasmas implies the validity of the Saha equation. Since the measured electron number density is much smaller than the atom number density, it can be taken to be equal to the number density of singly ionized Cs atoms. Therefore, the Saha equation for cesium can be written as

$$N_e = \sqrt{N_{Cs}} \times 10^{A(T_S)/2}, \tag{5}$$

where $A(T_S) = 15.383 + 1.50 \times \log T_S - 1.9621 \times 10^4 / T_S$. Here, T_S is the temperature in the Saha equation which, under the LTE conditions, should be equal to the temperature of the free electrons T_e, the Cs vapor temperature T_A, and the excitation temperature T_{exc}. The handy but accurate formula (5) which gives N_e in units of cm^{-3} is taken from [23].

It is easy to check that substitution of $T_S = T_{exc}$ and $N_{Cs} = N_{Cs}^{out}$ in Eq. (5) yields the electron number density of $N_e' = (7.9 \pm 2) \times 10^{14}\,cm^{-3}$, which is more than two times higher than the value measured here. However, there is excellent agreement with the result obtained from the Stark line broadening if the lower value $N_{Cs}^{in} = (2.5 \pm 0.3) \times 10^{16}\,cm^{-3}$ is taken into account. In turn, this confirms the estimated high vapor temperature value in the excitation volume and the achievement of a resonantly laser induced Cs plasma in complete LTE at about 2500 K.

An additional check of LTE conditions in this experiment was made by determining independenty electron plasma temperature from the analysis of the recombination continuum ocurring in the process $Cs^+ + e^- \rightarrow Cs(5D) + hc/\lambda$ ($\lambda < \lambda_{5D}$), where hc/λ_{5D} is the binding energy of the $5D$ level. This band extends from about 590 nm to lower wavelengths. The intensity of this band is given by $I(\lambda) \sim \lambda^{-3} \times \exp[(hc/k_B T_e)(\lambda^{-1} - \lambda_{5D}^{-1})]$ [21]. The analysis of the $5D$ band shape (data set M5, not shown here) in the region 520–590 nm yielded the electron temperature of about (2400 ± 200) K, which was in a very good agreement with the plasma temperature obtained via Boltzmann plot method (see Figs. 5-8).

3.2. Second part of the measurement: transition of a resonantly laser-excited Cs vapor to LTE plasma

The second part of the experiment was carried out at experimental conditions which allowed to monitor the stepwise transition of a resonantly laser-excited cesium vapor to a LTE plasma. These measurements were performed at cesium atom number densities lower than in the first part of the experiment. In addition, the pumping rates were varied. The laser wavelength was tuned in the blue Lorentzian wing of the Cs D2 line close to its center. In this case and for the applied laser detuning range (see Table 1) the pumping rate $\Pi(s^{-1})$ can be calculated using the following expression [24]:

$$\Pi \approx \frac{e^2 f_{D2}}{2mh} \frac{\lambda^5}{c^4} \frac{W_0}{\pi r_0^2} \frac{N_{Cs}\gamma}{(\Delta\lambda_L)^2}. \tag{6}$$

The value of the used self-broadening rate coefficient $\gamma = (1.1 \pm 0.15) \times 10^{-7}\,cm^3 s^{-1}$ is given in [25]. Inserting of the values for γ, W_0, r_0 and $\Delta\lambda_L$ from Table 1 into Eq. (6), yielded the pump powers applied that were in the range $10^5\,s^{-1}$ to $10^7\,s^{-1}$.

The measured line intensities are related to the averaged excited state number densities in the observed volume, i.e., to the integral values along a thin column at the position $z = y = 0$. The relative populations in higher excited states were determined in the same way as previously described. However, due to differences between spatial distributions of the atoms excited to the resonance states and those excited to higher lying states, Eq. (4) was corrected by multiplying the right hand side by a factor $\int H_\lambda(r)dr / \int H_D(r)dr$. Here, $H_\lambda(r)$ and $H_D(r)$ label the radial distributions obtained by Abel inversion from the measured distributions $F_\lambda(y)$ and $F_D(y)$, respectively. Generally

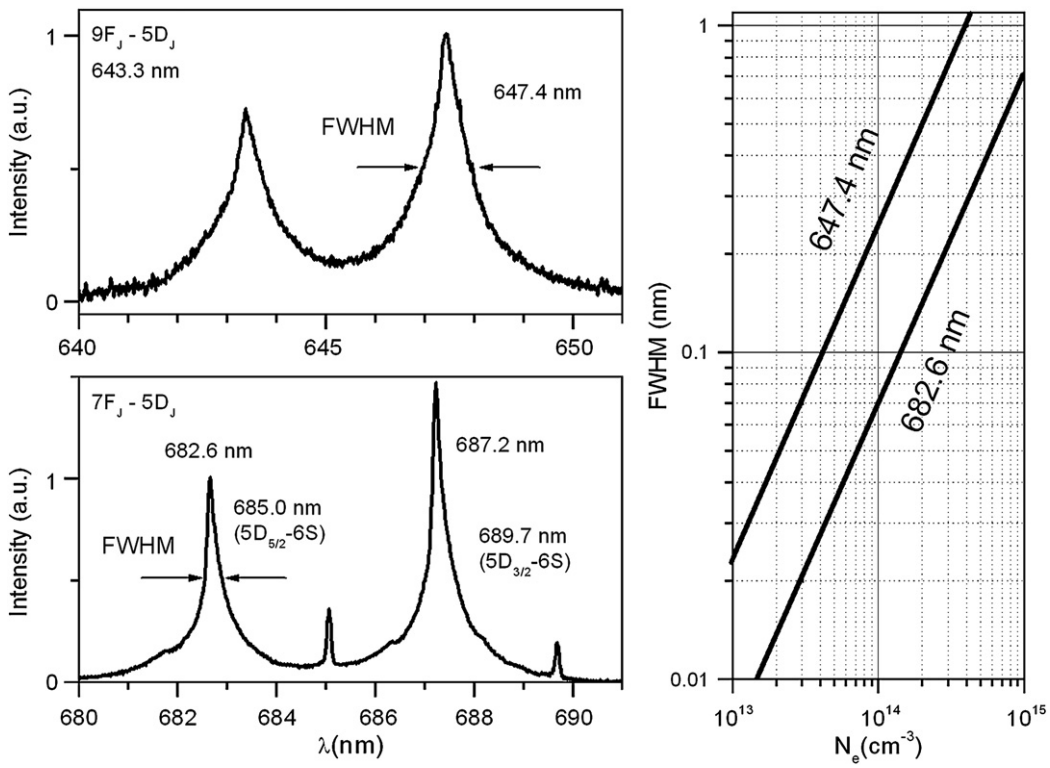

Fig. 6. Left: the Stark broadened Cs doublet lines of the Bergmann series. The spectra are enlarged parts of the spectrum displayed in Fig. 2. Right: the Stark widths (FWHM) of the $9F_J \rightarrow 5D_J$ and $7F_J \rightarrow 5D_J$ lines in dependence on electron density.

speaking, the intensity distributions $F_D(y)$ reflect the distribution product $N(6S, y) \times N(6P, y)$. The approximation was made because the gradient of the ground state atoms distribution $N(6S, y)$ is much smaller than the gradient of $N(6P, y)$, i.e., $F_D(y)$ was in practice directly related to the distribution of the atoms excited to the resonance states.

The Boltzmann plots comprising the relative populations obtained in the measurements M1, M3, M5, and M7 are given together with the data obtained in the first part of the experiment (M0) in Fig. 7. For the sake of the clarity of presentation, the data M2, M4, and M6 are omitted in the figure. Deviations from the straight-line dependence on energy for the particular data sets are represented by temperatures T_1 and T_2, which are defined as given in Fig. 7. The inset of Fig. 7 shows T_1 and T_2 as functions of the variable ΠN_{Cs}.

Absolute populations of the $6P_{3/2}$ state were determined form the measured optical depth $\tau(\nu) = \ln(I_0(\nu)/I(\nu))$ of the Cs 794.6 line obtained as explained in the previous section (see Fig. 4a). The probe beam was absorbed along the strongly inhomogeneous layer of the

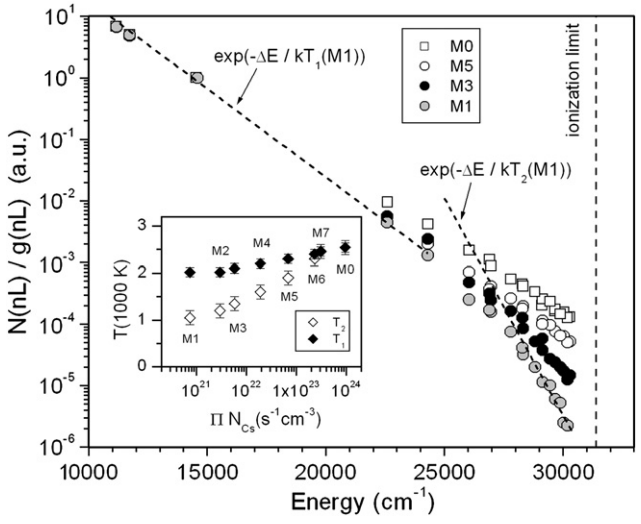

Fig. 7. Statistically weighted relative populations of the excited cesium states versus energy. The data are related to measurements performed in the second part of the experiment (M1, M3, M5, and M7). The data presented in Fig. 5 are plotted here too and labeled with M0. The "excitation" temperatures T_1 and T_2 are derived from partial Boltzmann plots restricted to lower and highly lying states. Their difference is a measure for the deviation from the Boltzmann distribution. Inset: temperatures T_1 and T_2 against the product of pumping rate Π and cesium number density N_{Cs}.

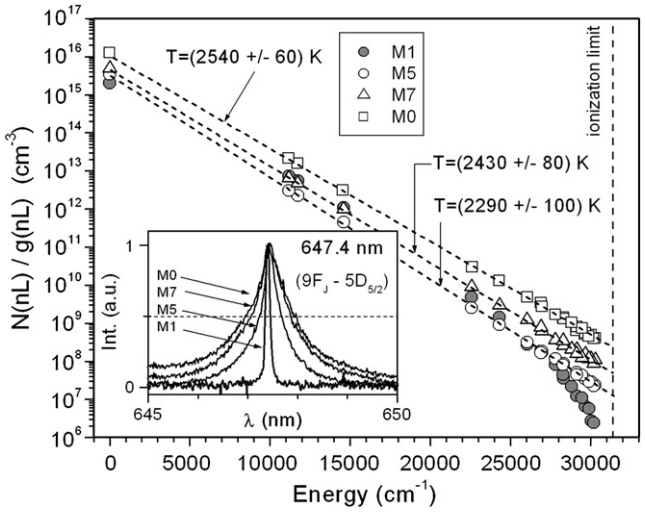

Fig. 8. Absolute values for statistically weighted relative populations versus energy obtained in the second part of the measurement (see M1, M5, and M7 in Table 1) together with data (M0) which are shown in relative scale in Fig. 5 as well as in Fig. 6. Inset: the Stark broadening of the Cs line at 647.7 nm yielding the information about the electron number density in the particular measurements.

atoms in the $6P_J$ state. The well-known Ladenburg relation is connecting the integral of the optical depth and the population $N(6P_{3/2})$:

$$\int \tau(\nu)d\nu = \frac{\pi e^2}{mc} f \int N(6P_{3/2}, z)dz, \quad (7)$$

where f is the line oscillator strength of the transition which is 0.021 [24]. The z-distribution of the $6P_{3/2}$ state atoms can be written as $N(6P_{3/2}, z) \approx N(6P_{3/2}, 0)\, F_D(z)$ if the same assumption as above is made. In that case, the $6P_{3/2}$ atom number density at the position $z=0$ can be obtained from the modified Eq. (7) as follows:

$$\int \tau(\nu)d\nu = \frac{\pi e^2}{mc} f N(6P_{3/2}, 0) L_{\text{eff}} \quad (8)$$

where the effective absorption length is given by $L_{\text{eff}} = \int F_D(z)dz$. The relative populations $N(nL)/g(nL)$ measured at the position $z=0$ have to be calibrated by the absolute $N(6P_{3/2})$ values in order to get their values in absolute scale.

In Fig. 8 three of seven sets of absolute statistically weighted populations are plotted versus energy. In addition, the figure displays the absolute populations obtained in relative scale in the first part of the experiment (see Fig. 5). The relative M0 data were converted to absolute values by making an extrapolation to $E=0$ and scaling them to the known ground state number density $N_{\text{Cs}}^{\text{in}}$. The inset of Fig. 8 displays the Stark broadening of the Cs $9F_J \rightarrow 5D_{5/2}$ line at 674.8 nm which was recorded in each of the measurements. In the measurements labeled by M7, M6 (not shown in Fig. 7) and M5, the Boltzmann plots are straight lines which show a systematic drop of the excitation temperature. The corresponding error bars progressively increase with the decrease of the excitation temperature. The measurements, labeled by M4, M3 and M2 in Table 1, are not included in Fig. 8 for the sake of clarity. There is an increasing deviation from the straight-line dependence which was most pronounced for the data obtained in the measurement M1.

As shown for T_1 and T_2 in Fig. 7, the regularities in the behavior of the particular measured quantities are best perceived if they are examined in dependence on variable ΠN_{Cs}. Note that $\Pi N_{\text{Cs}} \propto W_0\, N_{\text{Cs}}^2 / (r_0 \Delta\lambda_L)^2$. The electron number densities N_e, population densities $N(6P_{3/2})$ and the excitation temperature T_{exc} are shown as functions of the variable ΠN_{Cs} in the left plot of Fig. 9. At the lowest value of ΠN_{Cs}, i.e. in measurement M1, the Stark broadening of the $nF_J \rightarrow nD_J$ lines was too small to evaluate the electron number density. With increasing ΠN_{Cs}, the electron number density was measurable from the line width showing an increase of almost two orders of magnitude. The $N(6P_{3/2})$ number density, however decreased and had a minimum at $\Pi N_{\text{Cs}} = 10^{23}\,\text{s}^{-1}\,\text{cm}^{-3}$. This behavior indicates a strong de-excitation of the pumped resonance states which correlates with strongly increased electron number density. Beyond $\Pi N_{\text{Cs}} \approx 10^{23}\,\text{s}^{-1}\,\text{cm}^{-3}$ the $N(6P_{3/2})$ number density is increasing again. Consequently, the same dependence is observed in the "excitation" temperature T_3 which is related to the excitation of the resonant states and defined here as $T_3 = -[E(6P_{3/2}) / k_B] / \ln[0.5N(6P_{3/2}) / N_{\text{Cs}}^{\text{in}}(6S)]$, where k_B is the Boltzmann constant. The atom temperatures were determined in the same indirect way as presented in the measurement M0, i.e., by fitting the values $N_{\text{Cs}}^{\text{in}}$ in Eq. (4) in order to get correct values for $N(6P_J)/g(6P_J)$. It turned out that the differences between $N_{\text{Cs}}^{\text{in}}$ and $N_{\text{Cs}}^{\text{out}}$ were significantly smaller and more uncertain in the measurements M1–M5 than in all other measurements. This resulted in T_A values which were much lower and less accurate than those obtained in M6, M7, M8 and M0 measurements. Apparently, there is a large difference between the excitation and atomic temperature for $\Pi N_{\text{Cs}} < 10^{23}\,\text{s}^{-1}\,\text{cm}^3$. On the other hand, the difference between the excitation and atom temperature disappeared at the largest ΠN_{Cs} applied as Fig. 9 clearly shows. This means that the resonantly pumped Cs plasma approaches LTE conditions.

4. Discussion of the excitation and ionization processes

Numerous studies dealing with optically excited Cs vapors (see, for instance, [24] and references therein) have resulted with comprehensive set of relevant parameters for collisional transfer of electron energy among the excited cesium states. Based on these data, a clear picture can be obtained about main processes that govern the distribution of excitation energy among the excited states subsequent to initial laser

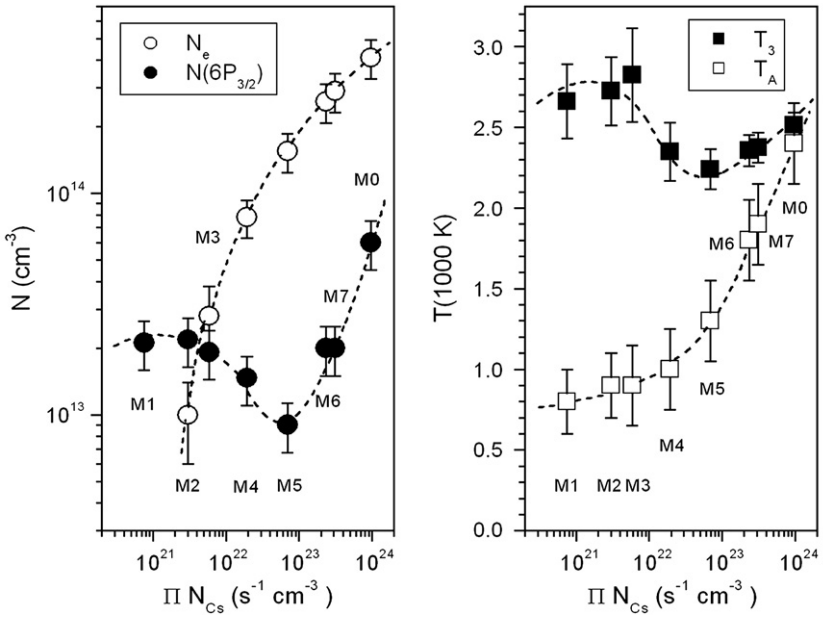

Fig. 9. Left: the measured electron number densities N_e and population densities $N(6P_{3/2})$ in dependence on the product of the relevant pump rates $\Pi(\text{s}^{-1})$ and cesium number densities N_{Cs} (cm^{-3}). Right: the excitation temperature T_3 related to the populations in the resonance $6P_J$ states and the estimated atomic temperatures T_A versus ΠN_{Cs}. See further explanations in text.

excitation of the resonant $6P_J$ states. The first and the most important process in further excitation (see Fig. 10) is quasiresonant energy pooling process:

$$Cs^*(6P) + Cs^*(6P) \xrightarrow{K_1} Cs^{**}(6D) + Cs(6S) + \Delta E(1), \quad (9)$$

in which two colliding cesium atoms excited to the 6*P* state produce one atom in the 6*D* state and the other atom in the ground state. The process (9) is exothermic and the average energy defect $\Delta E(1)$ amounts to $+479\ cm^{-1}$. In the conditions of the present experiment the populations in *J* states within the particular Cs nL_J multiplet are completely mixed due to collisions with ground state atoms. Therefore, in this consideration it is justified to describe the relevant collision processes in the simplified *J*-non-selective form (9). According to [20], the rate coefficient is $K_1 = 4.2\times10^{-10}cm^3s^{-1}$ at 570 K. The steady-state condition in the system is established through the radiative and non-radiative exchanges of the excitation energy with the neighboring levels, which can be described by following rate equation for the 6*D* state:

$$\frac{d}{dt}N(6D) = 0 = K_1N^2(6P) - N(6D)\sum_n R_{6D,nL} + \sum_n N(nL)R_{nL,6D} - N(6D)R_{PI}. \quad (10)$$

The first term in Eq. (10) describes the population of the Cs 6*D* state due to energy pooling. The rates $R_{6D,nL}$ in the second term represent all radiative and non-radiative (collisional) transitions from the Cs 6*D* state to the other states. In turn, the Cs 6*D* state is repopulated due to reverse processes, which is described by the third term with corresponding reverse rates $R_{nL,6D}$.

Additionally, there is the possibility of the photoionization process (not sketched in Fig. 10):

$$Cs^*(6D) + h\nu_L \rightarrow Cs^+ + e, \quad (11)$$

caused by photons of the laser pumping beam. This process is incorporated as fourth term in Eq. (10), where the photoionization rate is labeled with $R_{PI} = \Phi\sigma$. Here, Φ is the number of photons per unit time and unit area, while σ is the photoionization cross section. With the actual values for Φ (about $10^{19}cm^{-2}s^{-1}$) and the value $\sigma \approx 10^{-17}cm^{-2}$ [26], the photoionization rate R_{PI} is about 10^2s^{-1}, which is negligible in comparison with depopulation rates of the Cs 6D state in the second term of Eq. (10). On the other hand, the number density of electrons produced by the photoionization rate $R_{PI,}$ can be estimated from the following steady-state rate equation:

$$\frac{dN_e}{dt} = 0 = R_{PI}N(6D) - k_RN_e^2, \quad (12)$$

where k_R is the rate coefficient for radiative recombination. According to [27], the total radiative recombination rate coefficient to the ten lowest cesium states (processes: $Cs^+ + e \rightarrow Cs^*(nL) + h\nu$) at electron temperature of 2200 K amounts to about $5\times10^{-13}cm^3s^{-1}$. This, combined with typical number densities $N(6D) \approx 5\times10^{10}cm^{-3}$ measured in the present experiment, yields $N_e \approx 3\times10^{12}cm^{-3}$ as electron density produced by photoionization of the 6*D* state. This is only a very small fraction of the actual electron density measured.

A similar contribution to the total electron density can be expected from photoionization of the 7*P* state which is also populated by exothermic energy pooling process $Cs^*(6P) + Cs^*(6P)$ (see Fig. 10). However, to our knowledge, the corresponding rate coefficient has not been reported yet. An analysis which includes all other higher lying states shows that the production of free electrons by photoionization plays a minor role in the present experiment. Additional confirmation for this statement is given by the fact that the strong increase of the electron number density correlates with the drop of populations in all excited states which is contrary to expectation predicted by Eq. (12). This reduction of population (not plotted here) is analog to the population drop in the laser-excited state shown in Fig. 9.

Clear evidence that in the present experiment energy pooling of two $Cs^*(6P)$ atoms is the major mechanism for population of high-lying states is given by the observed spatial distributions of the excited atoms. As can be seen in Fig. 3a, for weaker laser pumping (M2), i.e., for lower values of ΠN_{Cs}, the spatial distribution F_D (representing the spatial distribution of $N(6P)$) extends far beyond the laser-excited zone. This is a consequence of the well-known trapping and "diffusion" of resonance radiation. In contrast to that, the distributions F_{685} (representing the spatial distributions $N(nL)$ of the atoms in higher excited states) are narrower but still broader than the laser beam. Data analysis yielded that for the spatial distributions measured in M1 (not shown here) and M2 a quadratic relationship $N(nL, y, z) \propto N^2(6P, y, z)$ is valid. This relationship fully agrees with the prediction given by expression (10). In addition, this relationship suggests that other possible processes involving only one Cs atom excited to 6P state and leading to the excitation of higher states in M1 and M2 are negligible in comparison with the $Cs^*(6P) + Cs^*(6P)$ energy pooling reactions. As shown in Fig. 3b, the differences between the relevant spatial distributions become smaller at higher values of ΠN_{Cs}. This effect correlates with the strong increase of the electron density (see Fig. 9) and it is obviously caused by strong intermultiplet mixing $Cs^*(6P) \Leftrightarrow Cs^*(nL)$ in collisions with electrons.

Simultaneously with de-excitation of 6*D* and 7*P* states, subsequent energy pooling processes occur, which involve cesium atoms excited to the 6P and 5D states:

$$Cs^*(6P) + Cs^*(5D) \xrightarrow{K_2} Cs^{**}(7D) + Cs(6S) + \Delta E(2) \quad (13)$$

$$Cs^*(5D) + Cs^*(5D) \xrightarrow{K_3} Cs^{**}(7F) + Cs(6S) + \Delta E(3) \quad (14)$$

The process (13) is exothermic ($\Delta E(2) = +38\ cm^{-1}$), while the process (14) is endothermic ($\Delta E(3) = -38\ cm^{-1}$). According to [20], the estimated values for the corresponding rate coefficients K_2 and K_3 amount to about $1.2\times10^{-9}cm^3s^{-1}$ and $8\times10^{-10}cm^3s^{-1}$, respectively.

The efficiency of energy pooling processes in the excitation of highly excited Cs states can be illustrated by the following example. In Fig. 11, the populations of the higher Cs states obtained in M1 experiment are compared with the data published in [20]. Both data

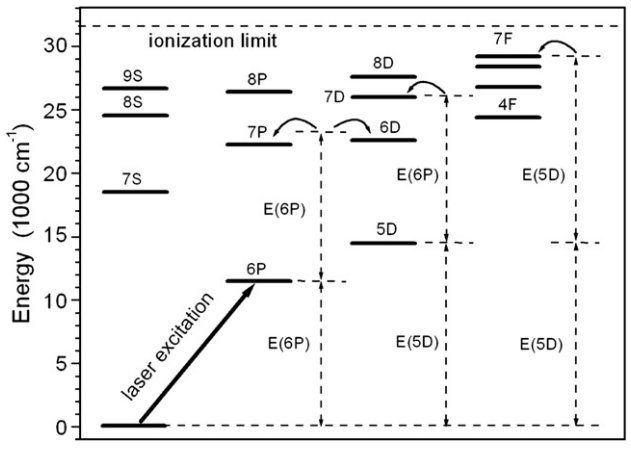

Fig. 10. Partial term diagram of cesium showing the major energy pooling excitation paths.

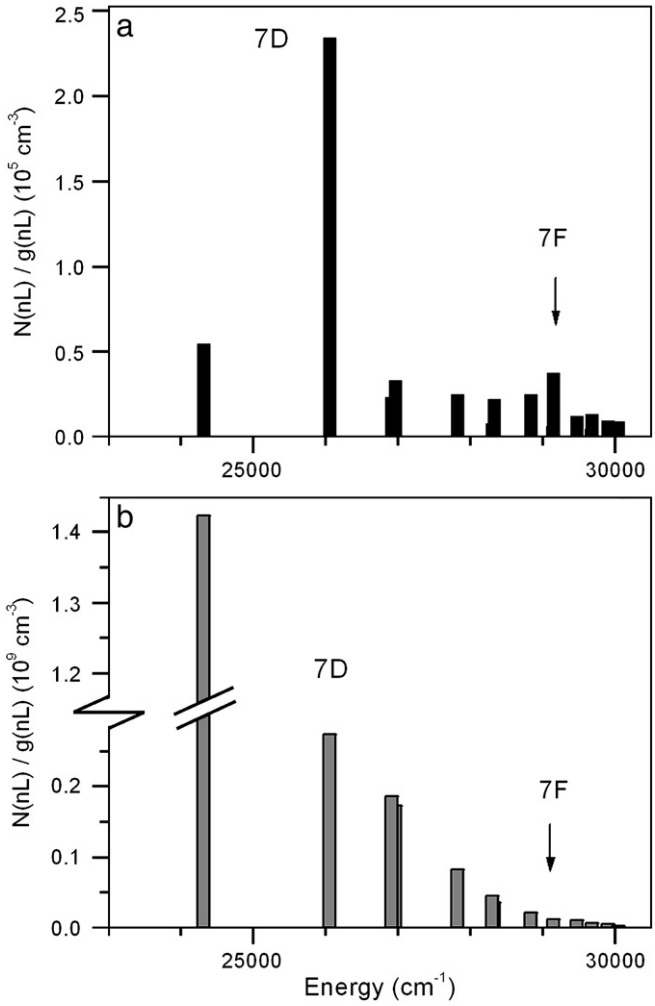

Fig. 11. (a) The statistically weighted absolute number densities vs. energy in the case of very weak pumping. The data are taken from Ref. [20]. (b) The same sequence measured here (M1). See text for further explanations.

sets were obtained at similar Cs vapor temperature (≈600 K) and number density (≈10^{16} cm^{-3}). However, the pumping of the Cs resonance states in the present investigation was several orders of magnitude stronger than in the measurement published in [20]. As can be seen in Fig. 11a, the weak pumping produces excess population in 7*D* and 7*F* states induced by energy pooling processes (13) and (14). The number density of electrons in that measurement was negligible and the populations in the neighboring states are produced by intermultiplet mixing with 7*D* and 7*F* states due to collisions with ground state atoms only. The number densities in 6*P* and 5*D* states in that measurement were 2.9×10^{11} cm^{-3} and 5×10^{10} cm^{-3}, respectively. In contrast to that, in the present experiment (M1, see Fig. 11b), the populations in the excited states produced even at lowest pumping in the present experiment (M1, see Fig. 11b) are much larger than in [20]. In addition, the populations measured in M1, as well as in the other measurements here, when plotted in dependence on the energy of the excited states, show a monotonous distribution in which the initial excess of population in 7D and 7 F states is obviously smoothed out. Since the ground state atom number densities are nearly the same in [20] as in measurement M1, one can conclude that this equalization is likely due to presence of charged particles. The actual electron density in M1 is obviously sufficient to produce collisional intermultiplet mixing as well as smoothing of the populations due to radiative recombination.

In the existing models, which describe the formation of plasma in the conditions similar to the ones in the present experiment, the excitation of the high-lying states and ionization are considered to occur through the superelastic collisions of slow electrons and excited atoms. This mechanism was proposed by Measures [5] to explain the pioneering work of Lucatorto and McIlrath [6]. Initially slow free electron (produced for instance by photoionization) increases his initial small kinetic energy ε by undergoing superelastic collision with excited atom

$$Cs^*(nL) + e(\varepsilon) \rightarrow Cs(6S) + e(\varepsilon + E_{nL}) \quad (15)$$

After one or more such superelastic collisions, the fast electron attains sufficient kinetic energy to excite the atoms in highly lying levels or to produce ionization:

$$Cs^*(mL) + e(\varepsilon + E_{nL}) \rightarrow Cs^+ + e(\varepsilon') + e(\varepsilon'') \quad (16)$$

After this ionization, there are two remaining slow electrons which undergo the same cycle. Numerous studies on ionization processes in laser-excited atomic vapors were performed, where either first resonance or higher lying states were excited by pulsed or cw lasers. It was shown [see, for instance, [9] and references therein] that the superelastic electron collisions become important above a certain input laser power threshold. Below this threshold a series of other mechanisms (photoionization, Penning ionization, and associative ionization) are responsible for production of free electrons.

It is interesting to compare the present results with those reported in [9] where the cesium vapors at similar conditions were excited by cw laser at the second resonant $6S \rightarrow 7P$ transition. In that measurement excitation temperatures of about 2050 K were achieved, while the electron densities, measured via broadening of $nF \rightarrow 5D$ lines too, were about 10 times lower than here. The maximum applied power of the broad-band ($\Delta_{laser} \approx 20$ GHz) multimode cw laser in [9] was about three times higher than in the work at hand. The complete LTE at about 2500 K obtained here is obviously due to very efficient absorption of the input single mode laser power at the first resonant transition. However, the measured absolute number densities of excited atoms show that the heating of cesium vapor and LTE plasma formation cannot be explained by the model of superelastic collisions of slow electrons and excited atoms. First of all, the maximum number density of free electrons measured in the present experiment amounts only to about 1% of the atom number density. As shown in Sections 3 and 4, the increase of electron density is correlated with the drop of the excited atom number density. Similarly as for previously considered photoionization, this population drop is in strong opposition with the model of "runaway" excitation and ionization due to superelastic electron collisions. In addition, the heating of atoms and realization of the complete LTE cannot be explained by superelastic electron collisions. It should be emphasized that the achievement of complete LTE in the present experiment is also confirmed by fulfillment of Griem's criterion [22]. A Cs plasma should be in complete LTE at $T = 2500$ K if the electron density is:

$$N_e(cm^{-3}) \geq 9 \times 10^{17} (k_B T / E_H)^{1/2} (E_{6P} / E_H)^3 = 1.3 \times 10^{14} \quad (17)$$

where E_H is the ionization energy of hydrogen. This criterion is fulfilled in the measurements M6, M7 and M0, as one can see from the data plotted in Fig. 9.

The alternative path for laser heating and ionization, which requires strong pumping and high ground state atom number density is a direct conversion of the excitation energy to the kinetic energy of the atoms through exothermic collisions of optically excited atoms. In the first phase subsequent to strong optical excitation of atoms, the pumping transition is almost saturated and there is a large number of excited atoms which undergo either the energy pooling collisions or

the superelastic collisions with the ground state atoms (atom impact de-excitation, self-quenching):

$$Cs^*(6P) + Cs(6S) \rightarrow Cs(6S) + Cs(6S) + E_{6P} \quad (18)$$

where the excitation energy is transferred to the kinetic energy of colliding atom pairs. The effects of exothermic collisions may be significant. For instance, an efficient heating of Li (2*P*) atoms up to 2000 K due to exothermic reverse energy pooling $Li^{**}(3D) + Li(2S) \rightarrow Li^*(2P) + Li^*(2P)$ has been reported in [28]. The influence of exothermic collisional processes on gas heating is demonstrated by a simple model applied to physical conditions in our experiment, which is elaborated in Appendix A. Starting point in this modeling is the fact that, on average, each atom undergoes exothermic collisions several times before leaving the laser excitation volume due to diffusion. This leads to cumulative transfer of relevant energy defects into the kinetic energy of colliding atoms. Expected increase of the atomic temperature is a sum of contributions due to particular exothermic collisional processes. Each particular contribution is proportional to the product of the number density in the initial excited state of the considered exothermic reaction, the relevant rate coefficient and the energy defect. It should be pointed out that, in general, the rate coefficients k and the corresponding energy defects ΔE are roughly related by $k \sim 1/\Delta E$, i.e., the products $k \times \Delta E$ are not extremely system-specific (see [24] and references therein). Therefore, similar contributions to the temperature increase due to exothermic collisions can be expected even for the processes characterized by strongly different values of ΔE. However, the number densities in the initial excited states are of crucial importance. In a statistical assembly of ground as well as excited state atoms, having strongly increased average kinetic energy, there is a certain number of atoms, which are capable of being ionized in further mutual collisions. Simultaneously, the free electrons produced in hot assembly of laser-excited atoms, cause a decrease of the population in the excited states by undergoing superelastic collisions, thus leading to equilibration of atomic and electron excitation temperatures. As one can see in Appendix A, this modeling yields a good qualitative agreement with the experimental findings.

5. Conclusion

Plasma formation in cesium vapor induced by a cw single mode laser beam tuned close to the center of the D2 line was investigated in dependence on vapor number density and absorbed laser power. The energy pooling processes were identified as major mechanisms for generating populations in highly excited states. Weakly ionized ($N_e / N_{Cs} \leq 10^{-3}$) non-equilibrium plasmas ($T_A < T_e \approx T_{exc} \leq 2200$ K) were produced at low and intermediate laser pumping (pumping rates $\approx 10^5$–$10^6 s^{-1}$) and lower Cs number densities (N_{Cs} up to 2×10^{16} cm^{-3}). The plasmas were found to be in complete LTE at temperatures between 2300 and 2500 K when strong resonance laser pumping (pumping rates: $\approx 10^7 s^{-1}$) was applied in vapors with cesium number densities larger than 4×10^{16} cm^{-3}.

The parameters of the non-equilibrium plasmas produced in lower pumping region were similar to those found in previous investigations (see [9] and references therein). According to [9], at non-LTE conditions, the electronic superelastic collisions seem to be the most important mechanism for producing and sustaining the laser induced plasmas. However, as shown here, a further increase of the absorbed laser power and the atom number densities indicates that other processes, which are much more efficient in regard to heating of heavy particles, become dominant for plasma formation. Here, the major role of collisions between electrons and excited atoms is not in heating of the atoms but rather in inducing of a strong mixing of populations in excited states. Simplified modeling of energy balance in exothermic collisions involving the laser-excited atoms shows qualitative agreement with experimental findings.

A concluding confirmation of the validity of the described model with the important role of exothermic collisions will be obtained by time resolved emission measurements which are under way in our laboratory.

Acknowledgements

Financial support by the Deutsche Forschungsgemeinschaft (DFG project: 436 KRO 113/9), the Ministry of Science, Education and Sports of the Republic of Croatia (project No. 035-0352851-2853), the Ministry of Innovation, Science, Research and Technology (State of North Rhine-Westphalia), and the Ministry of Education and Research (Federal Republic of Germany) are gratefully acknowledged.

Appendix A. The model of gas heating and ionization due to exothermic collisions

We consider only the cesium ground state 6*S* (state 1) and the first resonance state 6*P* (state 2) with the fine structure neglected. This simplification can be taken as justified, since most (about 90%) of the excited cesium atoms in our measurements are found to be in the $6P_J$ states.

A.1. Rate equation

Following the conditions of the present experiment, we consider the atoms continuously optically excited to the state *2* in an excitation volume, which is small compared with the rest of the atomic vapor volume. The surrounding metal vapor is in thermal equilibrium with the metal bath at constant pressure p and temperature T. In this two-level model, the total number density N of the atoms is the sum of the populations N_1 and N_2 in states 1 and 2. The relevant excitation and de-excitation rates are indicated in Fig. A1.

The laser pumping rate, spontaneous emission rate and stimulated emission rate are labeled with Π_{12}, A_{21}, and $(g_1/g_2)\,\Pi_{12}$, respectively. Here, the statistical weights are $g_1 = 1$ and $g_2 = 3$, and $\Delta E = E_{6P} = 11548$ cm^{-1}. The R_{21} is the self-quenching rate due to collisions with ground state atoms (see expression (18)). The R_{21} is the rate for the reverse process, i.e. the transition rate for the atom impact excitation. The rate R_{diff} symbolizes the losses of excited atoms by diffusion to the volume outside the excitation region. In Fig. A1 additional collisional rates Y_{21} and Y_{12} are also indicated. They will be specified and included in the later step of this modeling. With $C_{21} = R_{21} + Y_{21}$ and $C_{12} = R_{12} + Y_{12}$, the steady-state rate equation for the number density N_2 reads

$$\frac{dN_2}{dt} = 0 = (\Pi_{12} + C_{12})N_1 - \left(\frac{g_1}{g_2}\Pi_{12} + A_{21} + C_{21} + R_{diff}\right)N_2, \quad (A1)$$

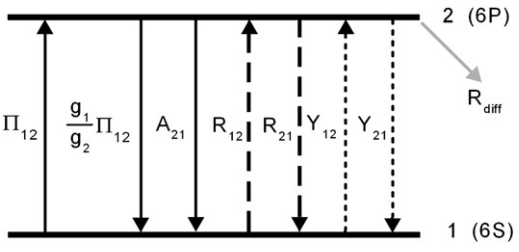

Fig. A1. Laser excitation of two-level atomic system used in the simplified model of Cs vapor heating due to exothermic collisions.

which in combination with $N = N_1 + N_2$ yields

$$N_2 = \frac{\Pi_{12} + C_{12}}{\Pi_{12}(1 + g_1/g_2) + A_{21} + C_{12} + C_{21} + R_{\text{diff}}} N \quad \text{(A2)}$$

The temperature-dependent quenching rate is given by $R_{21}(T) = Nk_{21}(T) = N_1\sigma_{21}(T)\, v_{av}(T)$, where $\sigma_{21}(T)$ is the corresponding cross section and $v_{av} = 1.8\times10^3\sqrt{T(\text{K})}\ \text{cm s}^{-1}$ is the average mean relative velocity between cesium atoms. The value $\sigma_{21} = 2\times10^{-16}\text{cm}^2$, measured at 635 K, can be found in reference [29]. According to the principle of detailed balancing, the atom impact excitation rate R_{12} is related to R_{21} through the expression $R_{12}(T) = R_{21}(T)(g_2/g_1)\exp(-E_{21}/kT)$. For instance, at low density and low temperature conditions present in our experiment ($N = 10^{16}\text{cm}^{-3}$, $T = 615$ K) the rate R_{21} amounts to $9\times10^5\text{s}^{-1}$ while R_{12} is extremely small ($5\times10^{-7}\text{s}^{-1}$).

The diffusion loses are determined by the diffusion coefficient D (units: cm^2s^{-1}) and the size of the excitation volume. According to the kinetic theory of gases, the pressure- and temperature-dependent diffusion coefficient is given by: $D(p,T) = D_0(p_0/p)\ (\text{T}/\text{T}_0)^{1.5}$. Here, D_0 is the diffusion constant for the given diffusion process at normal pressure p_0 and normal temperature T_0. Taking into account [30], the diffusion constant for Cs amounts to $8.3\times10^{-2}\text{cm}^2\text{s}^{-1}$. For the present geometry, the diffusion rate can be estimated via expression $R_{\text{diff}} \approx D[(2.4/r)^2 + (\pi/d)^2]$, where r and d are the average radius and length of the fluorescence zone [31]. At the low density and low temperature conditions specified above, the approximate value for R_{diff} amounts to 10^5s^{-1}.

The accurate value for the spontaneous emission rate A_{21} for the cesium first resonance transition is $2.7\times10^7\text{s}^{-1}$ [18]. However, at the present experimental conditions, the macroscopic A_{21} is reduced by radiation trapping and its effective value strongly depends on atomic number density and experimental geometry [24]. In the present case, as it will be shown below, the effective value for the A_{21} is estimated to be about $8\times10^6\text{s}^{-1}$.

A.2. Vapor heating and ionization

Besides the rate equation approach dealing with the population densities, one should carefully consider the energy exchange in the excitation volume and its balance with the vapor volume which is not interacting with the laser radiation. Here, it is important to identify the exothermic and endothermic processes in the rate equations and determine the change of the atomic kinetic energy. In the first step of our modeling (neglecting Y_{21} and Y_{12}) the products N_2R_{21} ($\text{cm}^{-3}\text{s}^{-1}$) and N_1R_{12} ($\text{cm}^{-3}\text{s}^{-1}$) in Eq. (A1) represent the numbers of exothermic and endothermic collisions per unit volume and unit time, respectively. Their difference divided by total number density N yields the net number of exothermic collisions B (s^{-1}) per one atom and per unit time

$$B = (N_2R_{21} - N_1R_{12})/N. \quad \text{(A3)}$$

Although negligible in the rate equation, the diffusion rate R_{diff} is crucial for an estimation of kinetic energy change of the atoms in the excitation volume. The time $\tau_{\text{diff}} = 1/R_{\text{diff}}$ is a measure for the average time which an atom spends a in the excitation zone before leaving it due to diffusion. Then, the quantity $B\tau_{\text{diff}}\Delta E$ is an average net change of the kinetic energy of a single atom in the excitation volume comprising $N/2$ homonuclear colliding atomic pairs. This means that, in contrast to the surrounding vapor being in thermal equilibrium and characterized by average atomic kinetic energy equal to $3k_BT/2$, the average kinetic energy of the atoms in the excitation volume is given by

$$E^{\text{in}} = \frac{3}{2}k_BT\frac{1}{2}B\tau_{\text{diff}}\Delta E \quad \text{(A4)}$$

The temperature T^{in} of the atoms in the excitation zone increases and becomes

$$T^{\text{in}} = T + \Delta T = T + \frac{B\tau_{\text{diff}}\Delta E}{3k_B} \quad \text{(A5)}$$

In the two-level model applied for $N = 10^{16}\text{cm}^{-3}$, $T = 615$ K and weak pumping ($\Pi_{12}/A_{21} = 0.1$), the expression (A5) yields the increase of the atomic temperature in the excitation zone $\Delta T \approx 5000$ K. However, in the steady-state regime, the excitation volume is in balance with the surrounding vapor, and the Dalton's law requires the pressure p^{in} in the excitation volume to be equal to the vapor pressure p. The number density N^{in} and temperature T^{in} in the excitation zone are related to the parameters N and T of the surrounding vapor by

$$N^{\text{in}}T^{\text{in}} = NT. \quad \text{(A6)}$$

This causes a decrease of excited atom number density and yields a lower steady-state change of the temperature than initially calculated. At stronger pumping and higher number densities the temperature increase calculated via Eq. (A5) is much higher than in the present example. At such high gas temperatures, electrons and ions are produced by collisions between fast atoms. Since the collisional processes in the present case are isotropic, it is plausible that the atoms in the excitation volume obey the Maxwell–Boltzmann velocity distribution. Consequently, one can introduce the Saha equation to estimate the corresponding number of ionized particles appearing due to fast atom–atom collisions. Saha equation is strictly valid only in thermal equilibrium, but it is justified to use it formally in the present modeling. Assuming that the excited state 2 is in LTE with the electron continuum, the relationship between the number density N_2^{in} in the excitation zone and electron density N_e [32] can be written in the following form

$$N_2^{\text{in}} = g_2(h^2/2\pi m k_B T_e)^{3/2}\exp(E_{\text{IP}}/k_BT_e) \quad \text{(A7)}$$

Here, the free electron temperature is labeled with T_e, while $E_{\text{IP}} = 19858\ \text{cm}^{-1}$ is the ionization potential of atoms in state 2.

Furthermore, the appearance of electrons requires considering their influence on the population in the excited state 2. This influence can be described by the rate Y_{21} for superelastic collisions (de-excitation by slow free electrons) and the rate Y_{12} for the reverse process, i.e., electron impact excitation by fast electrons. In general, the de-excitation rate can be written in the form $Y_{21}(T_e) = N_ek_{21}^{\text{SE}}(T_e) = N_e\sigma_{21}^{\text{SE}}(T_e)v_{\text{av}}(T_e)$. Here, the k_{21}^{SE} and σ_{21}^{SE} are the corresponding temperature-dependent rate coefficient and cross section, respectively, while $v_{\text{av}} = 6.1\times10^5\sqrt{T_e(\text{K})}\ \text{cm s}^{-1}$ is the average mean velocity of the electrons. Following the principle of detailed balancing, the rates Y_{12} and Y_{21} should be in the same ratio as previously given for the quenching rates R_{12} and R_{21}.

The theoretical simulation of our experimental results, which takes into account all assumptions and considerations given above, is presented in the next section.

A.3. Numerical simulations

In our calculations we define that $\Pi_{12}(\text{s}^{-1}) = 5\times10^5[N(\text{cm}^{-3})/10^{16}]$, which is an approximate relationship between the experimental pump rate and the actual vapor number density. The values of the rates R_{mn} and R_{diff}, are given in Sec. 5.1. We further assume that the relevant cross sections do not depend on temperature and we also assume that the diffusion rate has the simple form $R_{\text{diff}}(\text{s}^{-1}) = 10^5[10^{16}/N(\text{cm}^{-3})]$. Similar to the other simplifications made in the present semi-quantitative analysis, these approximations do not influence the final qualitative results. The parameters A_{21} and σ_{21}^{SE}, also needed for performing the calculations, were estimated using

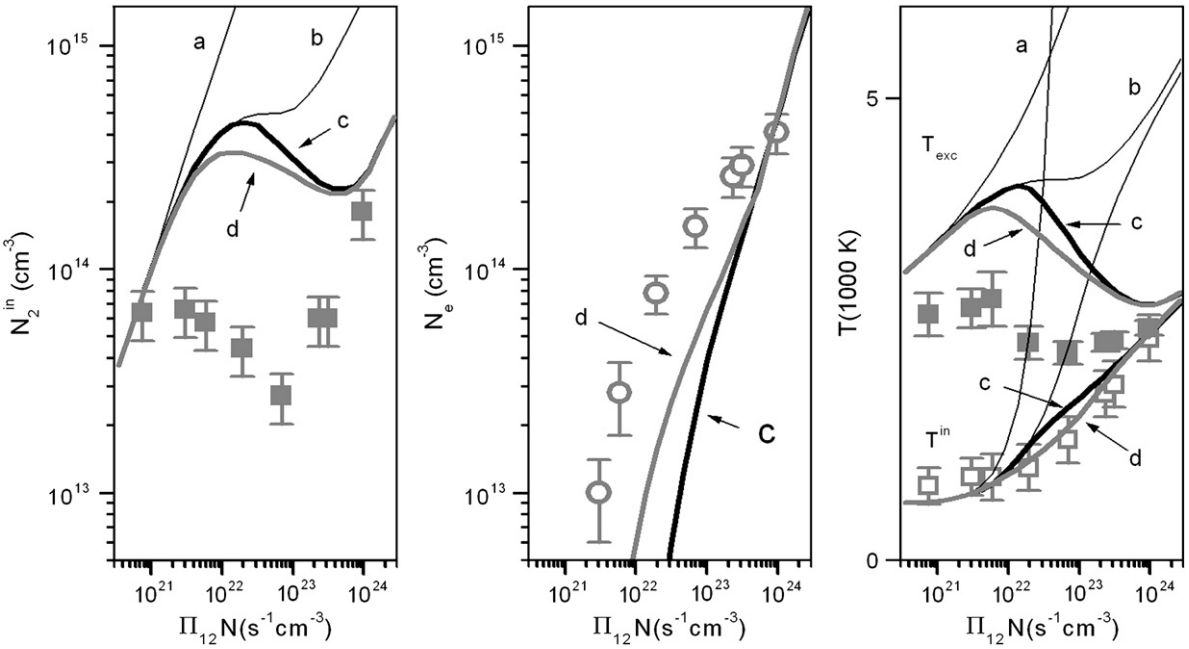

Fig. A2. The comparison of theoretical simulations (full lines) and experimental results (gray symbols). Labels a, b, and c, denote different two-level modeling: (a) based on basic rate Eq. (A1) only, (b) by including the Dalton's law, (c) by including both Dalton's law and Saha equation. In addition, the results for three-level modeling (case (d), gray lines) are plotted. Left: The calculated number densities N_2^{in} in the excitation zone and the measured $N_2^{exp} = N(6P_{1/2}) + N(6P_{3/2})$ versus the product of the pump rate $\Pi_{12}(s^{-1})$ and the number density $N(cm^{-3})$ of the atoms in the vapor. Middle: The calculated and measured electron number densities N_e versus $\Pi_{12}N$. Right: Theoretical and experimental values for excitation temperature T_{exc} and the atomic temperature T^{in} versus $\Pi_{12}N$. See further explanations in text.

rate Eq. (A1) and the experimental ratios N_2^{exp}/N_1^{exp}. From the data for lowest values for $\Pi_{12}N$, where Y rates can be neglected, one obtains $A_{21} \approx 8\times10^6 s^{-1}$. Using this value for A_{21} and the results obtained for the highest values for $\Pi_{12}N$, where Y rates become important, the estimated σ_{21}^{SE} is obtained to be about $2\times10^{-14}cm^2$ and the corresponding rate coefficient is $k_{21}^{SE} \approx 6\times10^{-7}cm^{-3}s^{-1}$. Here, the experimental values $N_e = 5\times10^{14}cm^{-3}$ and $T = 2500$ K were taken into account. It should be noted that the estimated super elastic collision parameters are of the typical order of magnitude (see, for instance [9] and references therein).

In Fig. A2 the experimental values for $N_2^{exp} = N(6P_{1/2}) + N(6P_{3/2})$, N_e and T, obtained from the data presented in Section 3 (Figs. 7–9) are plotted versus Π_{12} N together with the calculated values.

To demonstrate the influence of the particular mechanisms in our two-level model, the calculations were performed for three different cases: a) only basic rate Eq. (A1) was used for modeling, b) in addition to (A1) the Dalton's law was included, and c) both Dalton's law and Saha equation were considered together with the rate Eq. (A1). As can be seen in Fig. A2 (left), the calculated values for N_2 strongly disagree with the experimental values as the variable $\Pi_{12}N$ increases for case a). For the large values of $\Pi_{12}N$ the ratio N_2/N_1 approaches its maximum value $g_2/g_1 = 3$. In this limit, the excitation temperature $T_{exc} = -[\Delta E / k_B] / \ln[N_2 / 3N_1]$ becomes infinite and the temperature T^{in} calculated by Eq. (A5) tends to a high value (see curves (a) in Fig. A2 (right)), which eventually saturates. In the next step (case (b)), with $N_{in} = N_1^{in} + N_2^{in}$, the solution to the system of Eqs. (A1), (A5) and (A6) yields lower values for all calculated quantities. It should be noted that the inclusion of the Dalton's law in the consideration leads to T_{exc} and T^{in} which come close in value for the large $\Pi_{12}N$. This additionally supports the assumption that the Saha equation can be justifiably included in the calculations. Finally (case (c)), the system of Eqs. (A1), (A5)–(A7) with $N_{in} = N_1^{in} + N_2^{in}$ and additional condition $T^{in} = T_e$ yield the values for N_2^{in}, N_e, T^{in} and T_{exc} which are in good agreement with the experimental results obtained for high $\Pi_{12}N$-values.

Although the presented numerical simulations differ quantitatively from the experimental results in the intermediate range of $\Pi_{12}N$ values, it can be stated that the process of vapor heating by exothermic collisions is qualitatively well described by the model used.

As a step towards more elaborate modeling we have made an analysis based on three-level model. Without going into the details, we present also in Fig. A2 the results for the model comprising the 6S, 6P and 6D state (case (d)). In this simulation, the energy pooling process (9) was included in the appropriate set of rate equations and the corresponding contribution to the net number of exothermic collisions in Eq. (A5) was added. As can be seen in Fig. A2, the agreement between the calculated and experimentally obtained quantities has improved. More complex models require inclusion of additional levels and exothermic processes as well as the photoionization processes. Unfortunately, the lack of the data for collisional transition parameters needed in such numerical analysis leads to large uncertainties of calculated temperatures and number densities. In the presented simulations the process of the photoionization was excluded. The preliminary simulations within three-level model indicate that photoionization plays an important role only in the range of lower $\Pi_{12}N$ values.

Appendix B. Definitions and units

In the following, the notation, definitions and units of the physical quantities, used in this paper, are listed.

n	principal quantum number
L	orbital quantum number
L_{eff}	effective absorption length (m)
N_{Cs}	cesium ground state number density (m^{-3})
$N(nL)$	number density (m^{-3}) in the state characterized with quantum numbers n and L
N_e	electron number density (m^{-3})
$g(nL)$	statistical weight of nL state
$\Delta\lambda$	monochromator detuning from the line center (m)
$\Delta\lambda_L$	laser detuning from the line center (m)
$\delta\lambda$	monochromator band-pass (m)

$I_0(\nu)$ incident intensity (arbitrary units)
$I(\nu)$ transmitted intensity (arbitrary units)
$\tau(\nu) = \ln(I_0(\nu)/I(\nu))$ optical depth
$I(\Delta\lambda)$ wavelength dependent spectral intensity (arbitrary units)
W_0 power of the pump laser (W)
A Einstein coefficient for spontaneous emission, spontaneous emission rate (s^{-1})
$A(\Delta\lambda)$ spontaneous emission rate in the quasistatic resonance line wings ($cm^{-1}\ s^{-2}$)
R radiative or non-radiative (collisional) rate (s^{-1})
γ self-broadening rate coefficient ($s^{-1}m^3$)
k_R rate coefficient for radiative recombination ($s^{-1}m^3$)
Π_{12} pumping rate for the $1 \rightarrow 2$ transition (s^{-1})
Φ number of photons per unit time and unit area ($m^{-2}\ s^{-1}$)
σ cross section (m^{-2})
β detuning-dependent coefficient $m^3\ s^{-2}$)
$\varepsilon(\lambda)$ response of the detection system at the wavelength λ
T temperature (K)
h Planck constant (Js)
c velocity of light (ms^{-1})
k_B Boltzmann constant (J/K)
e electron charge (C)
m electron mass (kg)
f oscillator strength of the spectral line

References

[1] A. Rubenchik, S. Witkowski (Eds.), Physics of Laser Plasma, Handbook of Plasma Physics, vol. 3, North-Holland, Amsterdam, 1991.
[2] D. Bäuerle, Laser Processing and Chemistry, Springer Verlag, Berlin, 2000.
[3] D.A. Cremers, L.J. Radziemski, Handbook of Laser-Induced Breakdown Spectroscopy, John Wiley, Chichester, 2006.
[4] A.N. Nesmeyanov, Vapour Pressure of Chemical Elements, Elsevier, Amsterdam, 1963.
[5] R.M. Measures, Electron density and temperature elevation of a potassium seeded plasma by laser resonance pumping, J. Quant. Spectrosc. Radiat. Transfer 10 (1969) 107–125.
[6] T.B. Lucatorto, T.J. McIlrath, Efficient laser production of a Na^+ ground state plasma column: absorption spectroscopy and Photoionization measurement of Na^+, Phys. Rev. Lett. 37 (1976) 428–431.
[7] R.M. Measures, Efficient ionization of sodium vapor — a possible explanation based on superelastic collisions and reduced ionization potential, J. Appl. Phys. 48 (1977) 2673–2675.
[8] K.A. Menard, R.M. Measures, Superelastic collisional excitation of a strontium plasma by one- and two-photon laser pumping, Phys. Rev., A 35 (1987) 2330–2333.
[9] J. Huennekens, Z. Wu, T.G. Walker, Ionization, excitation of high-lying atomic states, and molecular fluorescence in Cs vapor excited at $\lambda = 455.7$ and 459.4 nm, Phys. Rev., A 31 (1985) 196–209.
[10] C.H. Greene, E.L. Hamilton, H. Crowell, C. Vadla, K. Niemax, Experimental verification of minima in excited long-range Rydberg states of Rb_2, Phys. Rev. Lett. 97 (2006) 2330021–2330024.
[11] G.C. Eiden, J.E. Anderson, N.S. Nogar, Resonant laser ablation: semiquantitative aspects and threshold effects, Microchem. J. 50 (1994) 289–300.
[12] C.G. Gill, T.M. Allen, J.E. Anderson, T.N. Taylor, P.B. Kelly, N.S. Nogar, Low-power resonant laser ablation of copper, Appl. Opt. 35 (1996) 2069–2082.
[13] D. Cleveland, P. Stchur, X. Hou, K.X. Yang, J. Zhou, R.G. Michel, Resonant laser ablation of metals detected by atomic emission in a microwave plasma and by inductively coupled plasma mass spectrometry, Appl. Spectrosc. 59 (2005) 1427–1444.
[14] S.L. Lui, N.H. Cheung, Minimally destructive analysis of aluminum alloys by resonance-enhanced laser-induced plasma spectroscopy, Anal. Chem. 77 (2005) 2617–2623.
[15] N.H. Cheung, in: A. Miziolek, V. Palleschi, I. Schechter (Eds.), Resonance-enhanced LIBS, in Laser-Induced Breakdown Spectroscopy: Fundamentals and Application, Cambridge University Press, 2006.
[16] W.L. Yip, N.H. Cheung, Analysis of aluminum alloys by resonance-enhanced laser-induced breakdown spectroscopy: how the beam profile of the ablation laser and the energy of the dye laser affect analytical performance, Spectrochim. Acta Part B 64 (2009) 315–322.
[17] V. Horvatic, M. Movre, R. Beuc, C. Vadla, The non-Lorentzian wings of alkali resonance lines: the determination of the atom number density in pure and mixed alkali vapours, J. Phys., B At. Mol. Opt. Phys. 26 (1993) 3679–3692.
[18] W. Hansen, The application of polarisation-influenced Thomas–Fermi ion models to alkali-atom transitions, J. Phys., B At. Mol. Opt. Phys. 24 (1984) 4833–4850.
[19] K. Niemax, Broadening and oscillator strengths of Cs quadrupole lines, J. Quant. Spectrosc. Radiat. Transfer 16 (1977) 125–129.
[20] C. Vadla, K. Niemax, J. Brust, Energy pooling in cesium vapor, Z. Phys., D At. Mol. Clust. 37 (1996) 241–247.
[21] L. Agnew, W.H. Reichelt, Identification of the ionic species in a cesium plasma diode, J. Appl. Phys. 39 (1968) 3149–3155.
[22] H. Griem, Plasma Spectroscopy, McGraw-Hill, New York, 1964.
[23] R.H. Curry, A spectroscopic study of low density cesium and cesium–helium discharges, J. Quant. Spectrosc. Radiat. Transfer 6 (1966) 357–367.
[24] C. Vadla, V. Horvatic, K. Niemax, Radiative transport and collisional transfer of excitation energy in Cs vapors mixed with Ar or He, Spectrochim. Acta Part B 58 (2003) 1235–1277.
[25] Z.J. Jabbour, J. Sagle, R.K. Namiotka, J. Huennekens, Measurement of the self-broadening rate coefficients of the cesium resonance lines, J. Quant. Spectrosc. Radiat. Transfer 54 (1995) 767–778.
[26] K. Gerwert, K.J. Kolath, Measurement of photoionisation cross sections for the $7^2P_{3/2}$ and $6^2D_{3/2}$ excited states of caesium, J. Phys., B At. Mol. Opt. Phys. 16 (1983) L217–L221.
[27] D.W. Norcross, P.M. Stone, Radiative recombination in cesium, J. Quant. Spectrosc. Radiat. Transfer 6 (1966) 277–290.
[28] D. Veza, C.J. Sansonetti, Ionization of lithium vapor by cw quasiresonant laser light, Z. Phys., D At. Mol. Clust. (1992) 463–470.
[29] M. Movre, V. Horvatic, C. Vadla, Caesium 6P fine-structure mixing and quenching induced by collisions with cesium ground-state atoms and molecules, J. Phys., B At. Mol. Opt. Phys. (1999) 4647–4666.
[30] A. Apelblat, P.S. Fialho, C.A. Nieto de Castro, The correlation of transport properties of alkali metal vapours, Fluid Phase Equilib. 227 (2005) 215–223.
[31] A.C.G. Mitchell, M.W. Zemansky, Resonance Radiation and Excited Atoms, University Press Cambridge, 1971.
[32] D.W. Norcross, P.M. Stone, Recombination, radiative energy loss and level populations in nonequilibrium cesium discharges, J. Quant. Spectrosc. Radiat. Transfer 8 (1968) 655–684.